The Glycophorin A Transmembrane Domain Dimer: Sequence-Specific Propensity for a Right-Handed Supercoil of Helices†

Herbert R. Treutlein,‡ Mark A. Lemmon, Donald M. Engelman, and Axel T. Brünger*

The Howard Hughes Medical Institute and Department of Molecular Biophysics and Biochemistry, Yale University, New Haven, Connecticut 06511

Received September 17, 1992; Revised Manuscript Received October 26, 1992

ABSTRACT: Recent studies suggest specific roles for transmembrane helix association in a range of functions, but understanding of the conformation and energetics of these interactions has been elusive. We have studied the specific dimerization of the transmembrane helix of glycophorin A by calculating the minimized interaction energies of a large number of conformations using simulated annealing techniques and tested the models against mutational analysis data. We find that the dimer is best modeled as a right-handed supercoil with an extensive region of close packing along the dimer interface. Furthermore, we observe a sequence-specific propensity for a right-handed supercoil to form when starting the simulated annealing modeling from a dimer of helices with parallel axes, in contrast with the dimerization region of the transcription factor GCN4 which shows a high propensity for the more prevalent left-handed supercoiling.

The transmembrane domains of many integral membrane proteins consist of one or more α-helices (Deisenhofer et al., 1985; Henderson et al., 1990; Gennis, 1989; Kühlbrandt & Wang, 1991; Lemmon & Engelman, 1992). Work on bacteriorhodopsin (Popot et al., 1987; Kahn & Engelman, 1992) and glycophorin A (Bormann et al., 1989; Lemmon et al., 1992a,b) has shown that association of transmembrane helices within single-chain proteins or oligomerization between several membrane proteins can be driven by sequence-specific helix–helix interactions. Furthermore, it now appears that the assembly of some membrane receptor complexes (most notably T-cell receptor and Fc receptors) is driven, at least in part, by interactions between the transmembrane domains of the constituent subunits (Manolios et al., 1990; Cosson et al., 1991; Kurosaki et al., 1991). Such interactions may include polar interactions within the membrane, packing effects, and constraints imposed by interactions outside the bilayer. The two-stage model of membrane protein folding (Popot & Engelman, 1990) postulates formation of independently stable hydrophobic helices across the lipid bilayer, followed by association or oligomerization. Apart from a structural role, such helix–helix association may be important for signal transduction across the membrane by some receptor proteins (Bormann & Engelman, 1992, Ullrich & Schlessinger, 1990; Milburn et al., 1991), oligomerization in the endoplasmic reticulum, and localization in different membrane compartments, as well as other functions (Lemmon & Engelman, 1992).

While ab initio prediction of protein structure is an elusive goal, the prediction of tertiary structure using procedures for docking elements of known secondary structure is more likely to succeed (Cohen et al., 1979). Thus, under the assumption of independently stable transmembrane helices (Popot & Engelman, 1990), the problem is simplified, and one can hope to dock preformed transmembrane protein helices. Although the general principles of protein association seem to be fairly well understood, the application of these principles to the prediction of specific association remains difficult even for a seemingly straightforward case. Simple criteria, such as buried surface area, solvation free energy, electrostatics, or packing, are insufficient to predict correct association while empirical energy functions are prone to inaccuracies and subject to the multiple minimum problem (Shoichet & Kuntz, 1991).

Under certain minimal assumptions about helix–helix association, it is possible to guide the docking process. In this paper we predict possible conformations of the dimer of the glycophorin A (GpA) (Welsh & Thom, 1985) transmembrane domain. Modeling was performed in two stages. First, in order to search for stable low-energy configurations of the dimer, the helix–helix interaction energies were calculated for the helices in a large number of different relative orientations. Each configuration was minimized by simulated annealing (Kirkpatrick et al., 1983) implemented as a combination of molecular dynamics simulations and energy minimizations. All possible symmetric and nearly symmetric arrangements of the pair of helices were thus studied. This approach identified essentially three likely low-energy configurations. To establish the convergence of the calculations, we also applied a different simulated annealing protocol which had been successful in predicting the coiled-coil configuration of the leucine zipper domain of the transcription factor GCN4 (Nilges & Brünger, 1991, 1992). In both protocols, molecular dynamics simulations used geometric (Brünger, 1991) and empirical energy functions (Karplus & Petsko, 1990) and were employed to overcome energy barriers between local minima, allowing convergence to lower minima than can be reached by conventional energy minimization.

Through a combination of these approaches, one low-energy configuration has been obtained in which the residues which lie at the helix–helix interface are identical to those which have been identified in the accompanying mutational analysis (Lemmon et al., 1992b). This structure consists of two α-helices in a closely fit right-handed supercoil. The mutagenesis and modeling studies were undertaken in parallel, and it is of note that modeling suggested the sensitivity of

† This work was funded in part by grants from the NATO Scientific Affairs Division managed by the DAAD (H.R.T.), the Howard Hughes Medical Institute (H.R.T., A.T.B., and M.A.L.), the Pittsburgh Supercomputer Center (A.T.B., DMB910036P), and the NIH (D.M.E., 5PO1GM39546). The predicted coordinates of GpA74–91 are available upon request from A.T.B.

* Author to whom correspondence should be addressed.

‡ Present address: Ludwig Institute for Cancer Research, P.O. Royal Melbourne Hospital, Parkville, Victoria 3050, Australia.

0006-2960/92/0431-12726$03.00/0

some of these interfacial residues to mutation before the experimental data were obtained.

MATERIALS AND METHODS

Molecular Dynamics Parameters and Restraints

All calculations, including the generation of initial structures, employed the X-PLOR program (Brünger, 1992) in conjunction with the parameter set PARAM19 (Brooks et al., 1983) with polar hydrogens included. A dielectric constant of $\epsilon = 1$ was chosen. Except otherwise noted, no screening or shifting function was applied to the electrostatic and van der Waals energy terms. The cutoff radius for the truncated nonbonded interactions was set to 15 Å for all cases except those that employed an r-dependent dielectric screening function in which case the cutoff was set to 9 Å.

Half-parabolic restraints were applied in all calculations that prevented the helix axes from separating by more than 10.4 Å (Nilges & Brünger, 1991). Distance restraints were applied to prevent breaking of the N–H···C–O hydrogen bonds in a helix. All simulations were carried out in vacuo to speed convergence. This is justified in part by the implicit modeling of environmental effects through the restraints and by the low dielectric environment within a membrane bilayer.

Initial Coiled-Coil Coordinates

The initial C^α coordinates for left- ($s = -1$) and right-handed ($s = +1$) supercoils were generated by transforming a single α-helix with ideal geometry using Crick's (1953) formula

$$x_i = r_0 \cos(t + \phi_i) + x_\alpha \cos(t + \phi_i) - y_\alpha \cos\omega \sin(t + \phi_i) \quad (1)$$

$$y_i = s r_0 \sin(t + \phi_i) + x_\alpha \sin(t + \phi_i) - y_\alpha \cos\omega \cos(t + \phi_i)$$

$$z_i = z_\alpha - y_\alpha \sin\omega$$

$$t = 2\pi z_\alpha / d$$

$$\omega = \arctan(2\pi r_0 / d)$$

where x_α, y_α, and z_α denote the coordinates of an ideal α-helix, i labels the helices A and B of the dimer, x_i, y_i, and z_i are the transformed coordinates, $r_0 = 5.2$ Å is the radius of the supercoil, $d = 186$ Å is the repeat distance, and ϕ_i describes the orientation of the helix with respect to the ideal helix. ϕ_i has been set to 0° and 180° for helices A and B, respectively.

Conformational Analysis

(*A*) *Definition of the Crossing Angle* Ω. Helical axes were defined by the average coordinates of the first seven and last seven C_α atoms for each helix. The points of closest approach (C_A and C_B) were determined for both axes. The crossing angle Ω was defined as the dihedral angle between the four points E_A, C_A, C_B, and E_B, where E_A and E_B are end points of the two helix axes.

(*B*) *Definition of the Shift.* The geometric centers of the 15 innermost C_α atoms were projected onto the diad axis of the supercoil. The shift was defined as the *absolute* difference between the projected centers.

(*C*) *Definition of the Separation between the Helices.* Distances were computed between geometric centers of a corresponding set of seven consecutive C_α atoms for both helices.

(*D*) *Definition of the Helical Configuration.* The C_α positions of the seven innermost residues of each helix were fitted separately to a reference structure by the method of Kabsch (1976). The angles α and β were defined as the axial rotation angles that produced the best fits to the reference structure.

(*E*) *Definition of the Helical Rise per Residue.* $d = \vec{a}[\vec{r}(C^\alpha_{m-3}) - \vec{r}(C^\alpha_4)]/(m - 7)$, where m is the number of residues of the helix, $\vec{r}(C^\alpha_i)$ is the coordinate of the C^α_i atom of residue i, and $\vec{a}$ is the helix axis.

(*F*) *Definition of the Number of Residues per Turn.* $n = 360(m-8)/\sum_{l=4}^{m-4}\Theta_{l,l+1}$, where $\Theta_{l,l+1}$ is the angle between the C^α_l position, the helix center, and the C^α_{l+1} position, projected onto a plane perpendicular to the helix axis (Chothia et al., 1977, 1981).

Simulated Annealing Protocols

Two types of simulated annealing protocols were performed in order to assess convergence. In the first type we started from initial C^α coordinates obtained from Crick's formula (eq 1) for a large number of left- and right-handed coiled-coil configurations. In the second type we started from uncoiled helices with parallel axes. Due to the larger motion necessary to accomplish supercoiling, this simulated annealing protocol is more computing intensive; therefore, we employed it only for a small number of low-energy configurations found with the simpler simulated annealing protocol.

Exhaustive Searches Starting from Coiled Coils

The initial left- or right-handed coiled-coil conformations described in eq 1 were used as starting and reference structures. Each of the two helices (A and B) was then rotated around its own helical axis by a certain angle: α for helix A and β for helix B. These rotations were achieved as follows: first, helix A was rotated around an axis defined by its first three C^α atoms by an angle α, while helix B remained fixed in space. This placed the residues of helix A in the desired relative orientation but destroyed the close contact between the two helices. This close contact was regained by optimization of the positions of the backbone atoms of helix A using energy minimization which employed as artificial distance restraints the conditions mentioned above for maintaining helical geometry and preventing the helices from dissociating (interactions for side-chain atoms were turned off during this minimization). After helix B had been rotated the same way by an angle β, a two-step energy minimization, including all atoms of both helices, was performed. This also allowed the side chains to reach conformations of minimum energy. In the first of these steps, side chains were treated as rigid bodies, and backbone atoms were fixed in a coiled-coil configuration. At this stage, only van der Waals and bond forces, as well as hydrogen bonds and the distance restraints between helix axes, were included. This minimization was used to remove bad contacts between side chains. When the van der Waals energy had dropped below zero, a second minimization was started, which included all interactions. Backbone atoms remained fixed, but all atoms were now treated individually. At this stage, all bad contacts had usually been removed, and the dimer was found to be in the desired conformation. In a few cases (fewer than 2%) bad contacts remained, and these initial configurations were either discarded or recalculated with slightly altered values for α and β. Each initial configuration (α, β) was then optimized by simulated annealing consisting of an initial energy minimization, followed by a 20-ps molecular

dynamics simulation and a final energy minimization. During this stage all atoms were allowed to move freely, although helical hydrogen bond restraints and restraints on the distance between helix axes were maintained (see above). This refinement allowed the dimer and all side chains to reach a more favorable conformation (α', β'), with a crossing angle Ω. These parameters were obtained from the final coordinate set as described above under Conformational Analysis.

Searches Starting from Uncoiled Helices

This protocol has been described in detail by Nilges and Brünger (1991). Starting from initial positions of C^α atoms of straight parallel helices, the remaining side-chain and backbone atoms were built, which is followed by minimization of all atomic coordinates using a simulated annealing algorithm. However, in contrast to this earlier work we started from ideal helices with 3.6 residues per turn. The multistage protocol was also slightly modified: the system was simulated for 20 ps during stage III, stage IV was omitted, and an unscreened electrostatic potential energy function with $\epsilon = 1$ was used.

Definition of Disruptive Mutants

Only conservative amino acid changes were considered for this estimate, i.e., mutations of side chains to one of the $N = 8$ amino acids A, C, V, L, I, M, F, or W of GpA (Lemmon et al., 1992a,b). A real number, s_{ik}, was defined to estimate the influence of a single-site mutation (k) for residue i. $s_{ik} = 1$, if the mutation was completely disruptive, $s_{ik} = {}^2/_3$, if a small amount of dimer was detectable, $s_{ik} = {}^1/_3$, if the protein remained mostly dimeric, and $s_{ik} = 0$, if no effect could be detected. The relative number of disruptive mutants P_i is defined as

$$P_i = (N/n_i)\sum_k s_{ik} \qquad (2)$$

where n_i is the total number of the observed mutations for residue i.

Interaction Energies

The interaction energies between helices were computed by summation of selected nonbonded terms of the empirical energy function (Brooks et al., 1983) involving pairs of atoms ij, where atoms i and j belong to helices A and B, respectively. The overall interaction energy was computed by summation of all nonbonded terms between both helices. The per-residue interaction energy was computed by summation of all terms ij, where i belongs to a particular residue of one of the helices and j can be any atom of the other helix.

RESULTS AND DISCUSSION

We used the following minimal assumptions about the structure of GpA which are borne out by studies of the specificity of association (Bormann et al., 1989; Lemmon et al., 1992a,b) and circular dichroism measurements (Welsh & Thom, 1985): the transmembrane GpA domains are α-helical, the helices are parallel (i.e., the peptide chains have the same directionality), and the helices are in contact throughout the membrane. We implemented these assumptions by restraining the α-helical backbone hydrogen bonds and applying a half-parabolic restraining potential to the local helix axes that prevents them from dissociating. In all calculations we simulated residues Thr-74 through Ile-91 (TLIIFGVMAGVIGTILLI) of GpA because they are well within the proposed membrane boundaries (Glu-72 and Tyr-93) of GpA (Welsh & Thom, 1985). We refer to this sequence as GpA74–91 in the following.

Early calculations on helix dimers over a wide range of values for α and β (data not shown) indicated that the search should be restricted to include only configurations near the axis of diad symmetry where $\alpha \approx \beta$. This indication was corroborated by the apparent pattern of sensitive residues in the accompanying mutational analysis (Lemmon et al., 1992b), which suggested that the same face of each helix was involved in the dimer interface. Furthermore, there is precedent for this in the cases of many other helical dimerization interfaces [e.g., in the catabolite gene activator protein (Weber & Steitz, 1987) and dimerization of the leucine zipper of GCN4 (Jones & Fink, 1982; Pathak & Sigler, 1992)].

Conformational space was sampled by creating families of structures using different initial random number seeds for the simulated annealing procedures and different relative orientations (which we refer to as configurations) of the helices. The spread of these families can be used to estimate the model's accuracy in a fashion similar to that employed for structure determination of macromolecules by solution nuclear magnetic resonance spectroscopy (Havel & Wüthrich, 1985; Clore & Gronenborn, 1991). In one set of calculations we started with ideal left- or right-handed supercoils (eq 1). In another set of calculations we started from a dimer of uncoiled helices with parallel axes; this starting model provides minimal bias toward either right- or left-handed supercoils.

Exhaustive Search Starting from Coiled Coils. Panels a and b of Figure 1 show the start and final configurations in the α,β plane obtained by the exhaustive search protocol (see Materials and Methods) starting from right- (Figure 1a) and left- (Figure 1b) handed coiled coils, respectively. It is clear that the final structures cluster in certain specific areas. For example, there appears to be some preference in the case of the right-handed supercoil for the regions around $\alpha = 90°$, $\beta = 90°$ and $\alpha = 300°$, $\beta = 300°$ in Figure 1a. By contrast, the region around $\alpha = 150°$, $\beta = 150°$ appears to be repulsive. These patterns result from ridges-into-grooves packing of the side chains (Chothia et al., 1977, 1981): certain configurations cause side chains to clash regardless of their rotamer conformations. The values and averages of the overall interaction energy between the two helices (the sum of the van der Waals and electrostatic interactions) are plotted as a function of the diadic angle $\phi = (\alpha + \beta)/2$ in Figure 1c for right-handed supercoils. A rather well-defined and highly populated minimum for the average interaction energy is seen close to the $\alpha = 90°$, $\beta = 90°$ configuration. In the case of the left-handed supercoils, attractive areas in the α,β plane also occur (Figure 1b), notably around $\alpha = 90°$, $\beta = 90°$, $\alpha = 250°$, $\beta = 250°$, and $\alpha = 300°$, $\beta = 300°$. The plot of the average interaction energy in this case (Figure 1d) shows two minima, around $\phi = 20°$ and $\phi = 275°$. However, these are rather less well populated than the right-handed $\phi = 90°$ energy minimum. Thus the search protocol identified three candidate best models with minimum average interaction energy. In each case, favorable electrostatic interactions made significant contributions to the low energy. Since these simulations were performed in vacuo, it was not possible to distinguish between these models without additional information.

Comparison with Mutational Analysis. To distinguish between the three possible models, we tested our predictions by comparison with the results of an extensive mutational analysis (Lemmon et al., 1992a,b). The shaded areas in Figure

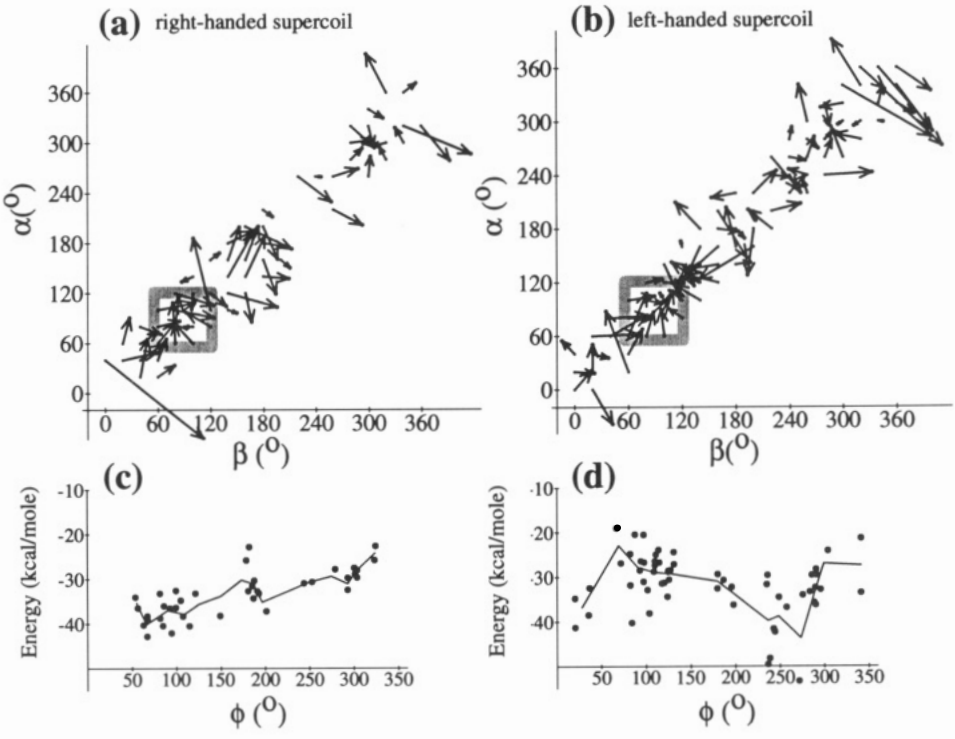

FIGURE 1: (a) Change of GpA74–91 configuration during simulated annealing starting from right-handed supercoils. (b) Same, starting from left-handed supercoils. (c) Final average interaction energies for the structures in (a). (d) Final average interaction energies for the structures in (b). Configurations are classified according to the two relative rotation angles, α and β (see Materials and Methods). The initial C^{α} coordinates were obtained from Crick's formula (eq 1) for a finite number of configurations (α, β), equally spaced around the diad axis (–40°, –20°, 0°, +20°, +40° for both α and β). Side chains were built in extended conformations and energy-minimized, and the whole structure was further refined by simulated annealing which consisted of 20-ps molecular dynamics simulations at 300 K followed by minimization (see Materials and Methods). The arrows in (a) and (b) indicate the initial and final configurations for each simulated annealing run. The shaded areas in (a) and (b) indicate the configurations that orient the most mutation-sensitive residues (Lemmon et al., 1992a,b) toward the dimeric interface. Overall interaction energies were computed by summation of the van der Waals and electrostatic energy terms between both helices (see Materials and Methods). Dots in (c) and (d) indicate the overall interaction energies for all simulated annealing runs as a function of the diadic angle $\phi = (\alpha + \beta)/2$; the solid line indicates a running average computed over a 20° wide window.

1a,b indicate the configurations that are most compatible with the mutagenesis data, i.e., configurations with the most sensitive residues at the dimerization interface. The shaded area for right-handed configurations is close to the global minimum of the average interaction energy (Figure 1a,c) and that for left-handed configurations is close to the global maximum. Thus, the right-handed configurations may be more "likely" only in the sense that many more structures can be found with low energies and agreement with the mutagenesis data than left-handed configurations. Clearly, this result does not rule out the existence of a left-handed supercoil.

For further testing, we compared the average interaction energies vs residue number and the mutagenesis sensitivity profile (Figure 2). In addition to occurring in an apparent global energy minimum for right-handed supercoils, an average of configurations occurring around $\alpha = 90°, \beta = 90°$ (Figure 2a) seems to agree remarkably well with the dimer interface suggested in the accompanying paper (Lemmon et al., 1992b). The model predicts strong interactions with the opposing helix for the same residues at which conservative substitutions disrupt the dimer of GpA74–91, as well as the helical periodicity of these residues (about 3.9 residues per turn, as would be expected for the interface of a right-handed supercoil). It is of note that this comparison was made before any mutational data had been obtained for Thr-87 or Leu-75, both of which are positions where substitution with hydrophobic residues disrupted the dimer considerably (Lemmon et al., 1992b). By contrast, averages from the left-handed supercoiled configurations (Figure 2c,d) do not agree particularly well with the mutagenesis data. These two comparisons show agreement only for the C-terminal and N-terminal half of the helix, respectively. In both cases, predicted sites of interaction are out of phase with the mutagenesis data over the remaining half of the helix. In addition, both predict only 3.5 residues per turn (as expected for a left-handed coiled coil), which differs from the value obtained in the mutational analysis. Furthermore, the average crossing angle Ω for the left-handed configurations is 55°, which is outside the range of classical coiled coils (Crick, 1953) and is rarely observed in proteins (Chothia et al., 1977, 1981). Thus these results lend more credibility to our suggestion that GpA74–91 dimerizes as a right-handed supercoil.

A comparison of the families of structures generated using the procedure of Nilges and Brünger (1991) from the initial uncoiled α-helices with the data from the mutational analysis (Figure 2b) gives essentially the same agreement, lending further credence to the results obtained using our exhaustive search protocol above. Indeed, this comparison shows that rather similar structures which agree with the mutational analysis can be arrived at using different methods and starting with rather different initial structures.

Preference for Right-Handed Supercoiling of GpA74–91. There is a strong preference for right-handed supercoiling when the simulated annealing modeling is started from an uncoiled conformation (Figure 2b). Of 20 structures generated with this method, 17 formed right-handed supercoils and just 3 formed left-handed supercoils. The question arises as to whether this preference results from the relatively short GpA74–91 transmembrane segment of about 18 residues or

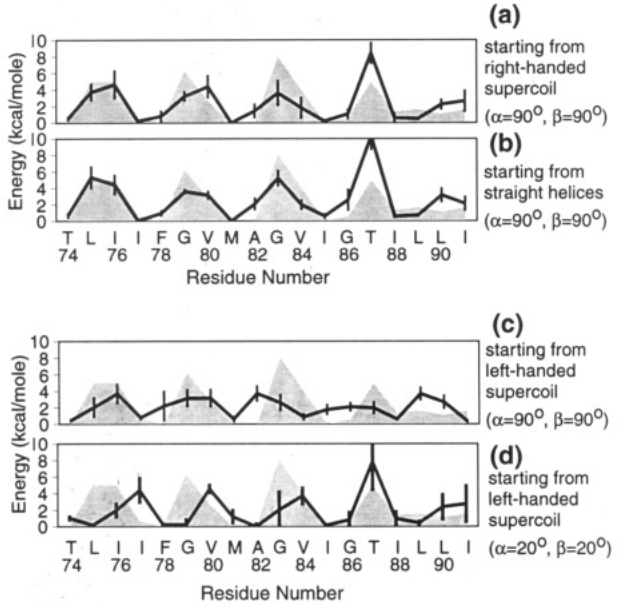

FIGURE 2: Comparison of average interaction energies vs residue number with the mutational sensitivity profile of GpA (Lemmon et al., 1992a,b) for a number of model structures. The shaded areas indicate the relative number, P_i, of disruptive mutants vs residue number as observed in the mutagenesis experiments (cf. Materials and Methods). The solid lines indicate interaction energies vs residue number (see Materials and Methods) averaged over both symmetric arrangements of the helices and over the corresponding families of simulated annealing structures. The bars indicate standard deviations of the interaction energies. (a) Models obtained by starting from those right-handed configurations that converged to the shaded area near $\alpha = 90°, \beta = 90°$ in Figure 1a. (b) Models obtained by starting from uncoiled dimers close to the configuration $\alpha = 90°, \beta = 90°$. The simulated annealing protocol employed the method by Nilges and Brünger (1991) modified as described under Materials and Methods. (c) Models obtained by starting from those left-handed configurations that converged to the shaded area in Figure 1b near $\alpha = 90°, \beta = 90°$. (d) Models obtained by starting from left-handed configurations near $\alpha = 20°, \beta = 20°$; we chose this orientation as it was relatively close to the shaded area allowed by the mutagenesis data, and the average interaction energy assumed a local minimum (Figure 1b,d).

is due to artifacts in the simulation. We addressed this question by the following "computer experiment": the GpA74–91 sequence was "mutated" into the 18-residue fragment Lys-7 through Glu-24 (KQLEDKVEELLSKNYHLE) of the leucine zipper domain of the transcription factor GCN4 (Jones & Fink, 1982; Pathak & Sigler, 1992) which forms a classical left-handed coiled coil in solution and in the crystal structure (O'Shea et al., 1991). Simulations in vacuo were started with uncoiled configurations just as with the GpA74–91 sequence. Figure 3 reports the crossing angles and shifts. It appears that even the shortened GCN4 sequence has a strong preference for left-handed supercoils while GpA74–91 has a strong preference for right-handed supercoils. As the preference of GpA74–91 appears to be largely independent of modifications of the electrostatic potential energy function (Figure 3), we conclude that it is driven by packing interactions and probably not influenced by the environment. The GpA74–91 structures exhibit an average crossing angle of –30° and an average shift of 2 Å. Apparently, a relative displacement of the helices is required for optimal packing of the right-handed supercoils under the assumptions and approximations made. All right-handed configurations of GpA74–91 fall into the 4-4 class of helix packing (Chothia et al., 1977, 1981).

Analysis of the Predicted GpA74–91 Structure. Families of predicted GpA74–91 structures starting from right-handed supercoils and from uncoiled dimers are plotted in panels a

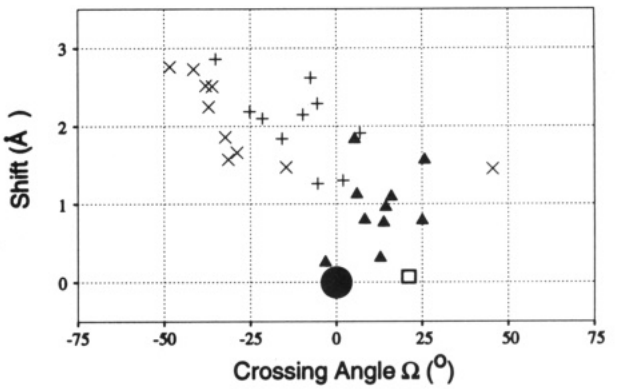

FIGURE 3: Scatter plot showing crossing angles and shifts for models obtained by starting from uncoiled dimers of ideal helices using the sequence of GpA74–91 and the shortened 18-residue fragment of the GCN4 leucine zipper (see text). The GpA74–91 calculations employed an unscreened electrostatic potential energy function (crosses) as well as an *r*-dependent dielectric screening function (pluses) to test the dependence on electrostatics in the calculations. The GCN4 calculations employed an *r*-dependent dielectric screening function as was done in previous work (Nilges & Brünger, 1991). Starting configurations were close to $\alpha = 90°, \beta = 90°$ for GpA74–91 and close to the X-ray crystal structure for GCN4 (O'shea et al., 1991). In contrast to previous work (Nilges & Brünger, 1991) we started from ideal, uncoiled helices with 3.6 residues per turn. Symbols: (×) GpA74–91, starting from straight helices, no screening; (+) GpA74–91, starting from straight helices, *r*-dielectric; (▲) GCN4, starting from straight helices; (□) GCN4, X-ray structure; (●) initial structures.

and b of Figure 4, respectively. A particular structure of the latter family is shown in Figure 4c. The rms deviation from the mean positions of the backbone (non-hydrogen) atoms disregarding the first three and last three residues for the structures in Figure 4a is 0.83 (1.76) Å while that for the structures in Figure 4b is 0.83 (1.78) Å. The average rms deviations between the two families of structures is 1.26 (2.67) Å, while the average rms difference between the initial structures (preformed right-handed supercoils around the $\alpha = 90°, \beta = 90°$ configuration vs the uncoiled dimer) is 1.64 (2.84) Å. Thus, the two families do converge to some degree during our simulated annealing procedure.

The average number of residues per turn for the single helices and the helical rise of the predicted structures are $n = 3.57 \pm 0.04$ and $d = 1.52 \pm 0.03$ Å, respectively. The average separation between helix axes is 7.95 ± 0.27 Å, which is significantly smaller than that found for the GCN4 simulations (9.76 ± 0.24 Å) and the GCN4 crystal structure (9.3 Å; O'shea et al., 1991). The closest contact between the GpA74–91 helices is near Gly-79 (≈6.9 Å), a region of high sensitivity in the mutational analysis, while the C- and N-terminal ends are further apart (≈9 Å at the C-terminus and ≈7.5 Å at the N-terminus). Of particular interest is the formation of an interhelical hydrogen bond between atom $O_{\gamma 1}$ of Thr-87 and $H_{\gamma 1}$ of Thr-87 of the opposite chain (Figure 4c). This hydrogen bond is formed in about 66% of all right-handed supercoil configurations that we obtained by the various calculations, and substitutions at Thr-87 can disrupt the dimer (Lemmon et al., 1992b).

CONCLUSION

The propensity for the GpA transmembrane dimer to form a right-handed helical supercoil clearly emerges from our calculations. As this propensity is largely independent of modifications of the electrostatic potential energy function (Figure 3), we conclude that it is driven by packing interactions at the dimer interface. It is possibly mediated in part by the

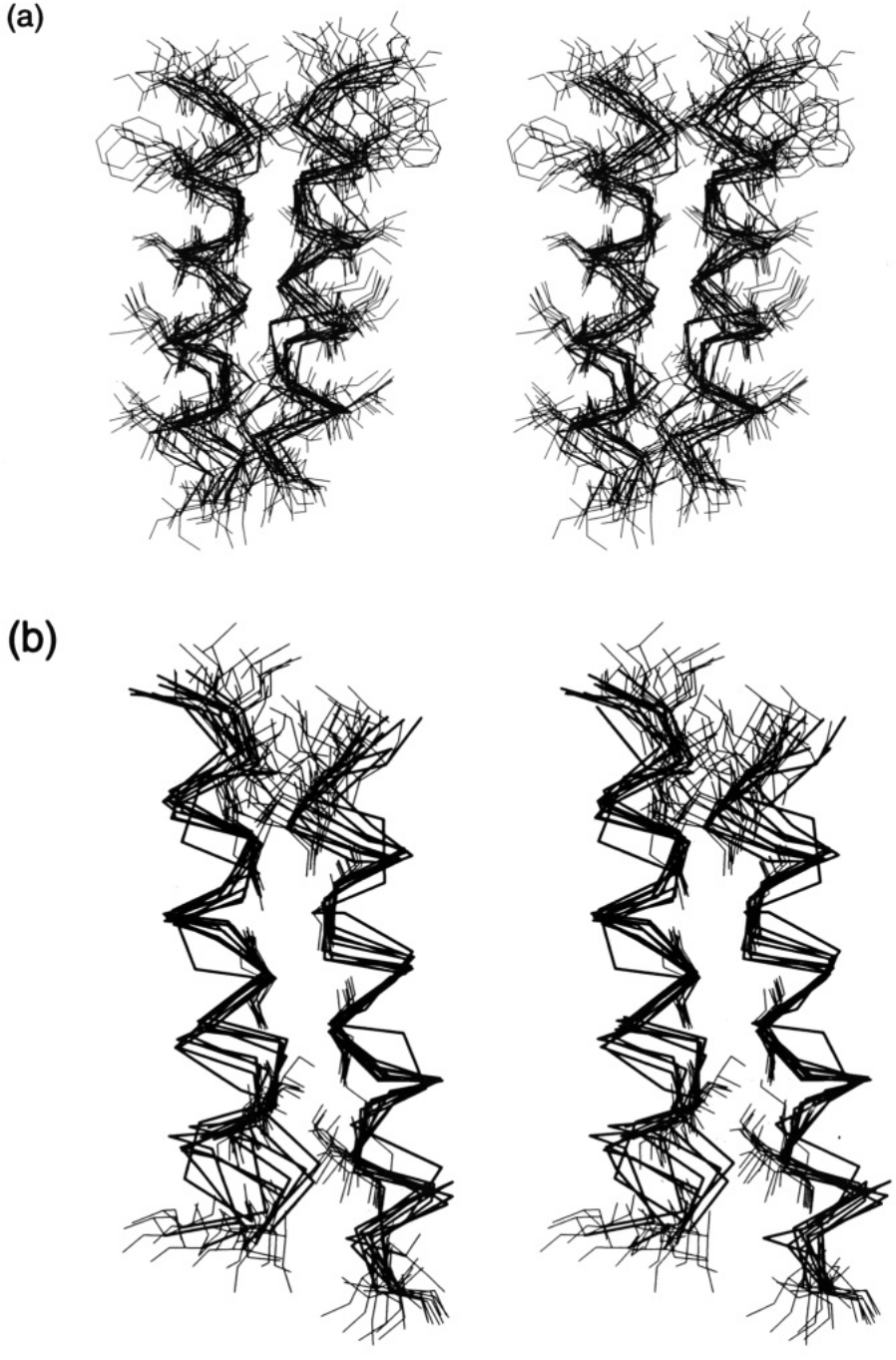

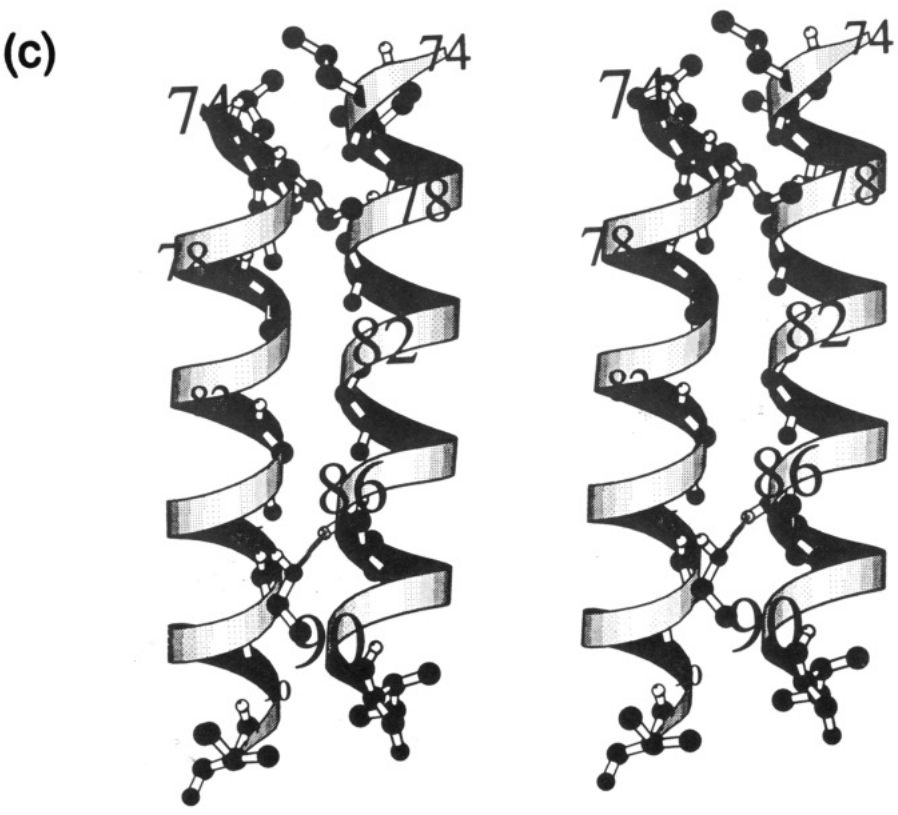

FIGURE 4: (a) Family of nine predicted GpA74–91 structures obtained by simulated annealing starting from those right-handed configurations that converged to the shaded area in Figure 1a near $\alpha = 90°$, $\beta = 90°$. The backbone is shown in thick lines while the side chains are shown in thin lines. (b) Final structures after stage III of the simulated annealing procedure. The starting structures consisted of dimers of ideal, uncoiled helices with configurations near $\alpha = 90°$, $\beta = 90°$. An unscreened electrostatic potential energy function was used. (c) Single structure drawn from this family. The hydrogen bond between $O_{\gamma 1}$ of Thr-87 on one helix and $H_{\gamma 1}$ of Thr-87 on the opposite helix is indicated by a gray line. Structures were superimposed by a least-squares method (Kabsch, 1976); helices were matched A → A and B → B or A → B and B → A, whichever produced a better fit. The MolScript program (Kraulis, 1991) was used for the graphical displays.

presence of two crucial glycine residues at the helical interface (Figure 4b). Indeed, the two helices approach one another closely around the helical turn separating Gly-79 and Gly-83 of GpA74–91. It should be noted that these glycines are among the most sensitive residues in the mutational analysis.

Helical supercoils are usually found in the standard left-handed coiled-coil conformation (Crick, 1953; Chothia et al., 1977, 1981; Cohen & Parry, 1990). However, Crick (1953) also suggested the possibility of a right-handed helical interaction; by applying a rigid knobs-into-holes packing scheme, he proposed crossing angles of $\Omega = 20°$ for left-handed coiled coils and $\Omega = -70°$ for right-handed helical interactions. A wide range of positive and negative values of Ω has actually been found in crystal structures (Chothia et al., 1977, 1981; Richmond & Richards, 1978) which can be understood in terms of a more flexible ridges-into-grooves packing scheme; out of 50 helix–helix packings observed in ten globular proteins, 25 were found to be right-handed ("class 4-4"). A recent electron crystallographic study of the pea light-harvesting complex shows low-resolution contours of a right-handed supercoil of parallel transmembrane α-helices in the center of the complex (Kühlbrandt & Wang, 1991).

The predictive ability of our simulated annealing approaches to modeling might be applicable to determine the handedness and conformation of other folding motifs such as α-helical bundles or β-sheets.

Our findings support the hope of predicting folded transmembrane protein structures in the hydrophobic region of the lipid bilayer. Basically only three models were arrived at by assuming the two-stage model of membrane protein folding and by applying global search and simulated annealing methods. Only one of them, the right-handed supercoil, was compatible with the mutagenesis data. It is conceivable that a more complete modeling of the bilayer environment and more accurate empirical energy functions could distinguish between the three models.

ACKNOWLEDGMENT

We thank M. Nilges, T. Simonson, D. Pathak, and P. Klosterman for helpful discussions.

REFERENCES

Bormann, B.-J., & Engelman, D. M. (1992) *Annu. Rev. Biophys. Biomol. Struct. 21*, 233–242.

Bormann, B.-J., Knowles, W. J., & Marchesi, V. T. (1989) *J. Biol. Chem. 264*, 4033–4037.

Brooks, B. R., Bruccoleri, R. E., Olafson, B. D., States, D. J., Swaminathan, S., & Karplus, M. (1983) *J. Comput. Chem. 79*, 187–217.

Brünger, A. T. (1991) *Annu. Rev. Phys. Chem. 42*, 197–223.

Brünger, A. T. (1992) *X-PLOR, Version 3.1, A System for X-ray Crystallography and NMR*, Yale University Press, New Haven, CT.

Chothia, C., Levitt, M., & Richardson, D. (1977) *Proc. Natl. Acad. Sci. U.S.A. 74*, 4130–4134.

Chothia, C., Levitt, M., & Richardson, D. (1981) *J. Mol. Biol. 145*, 215–250.

Clore, G. M., & Gronenborn, A. M. (1991) *Science 252*, 1390–1399.

Cohen, C., & Parry, D. A. D. (1990) *Proteins 7*, 1–15.

Cohen, F. E., Richmond, T. J., & Richards, F. M. (1979) *J. Mol. Biol. 132*, 275–288.

Cosson, P., Lankford, S. P., Bonifacino, J. S., & Klausner, R. D. (1991) *Nature 351*, 414–416.

Crick, F. H. C. (1953) *Acta Crystallogr. 6*, 689–697.

Deisenhofer, J., Epp, O., Miki, K., Huber, R., & Michel, H. (1985) *Nature 318*, 618–624.

Gennis, R. B. (1989) in *Biomembranes*, Springer Verlag, New York.

Havel, T. F., & Wüthrich, K. (1985) *J. Mol. Biol. 182*, 281–294.

Henderson, R., Baldwin, J. M., Ceska, T. A., Zemlin, F., Beckmann, E., & Downing, K. H. (1990) *J. Mol. Biol. 213*, 899–929.

Jones, E. W., & Fink, G. R. (1982) in *The Molecular Biology of the Yeast Saccharomyces: Metabolism and Gene Expression* (Strathern, J. N., Jones, J. N., & Broach, J. R., Eds.) pp 181–299, Cold Spring Harbor Laboratory, Cold Spring Harbor, NY.

Kabsch, W. (1976) *Acta Crystallogr., Sect. A 32*, 922–923.

Kahn, T. W., & Engelman, D. M. (1992) *Biochemistry 31*, 6144–6151.

Karplus, M., & Petsko, G. A. (1990) *Nature 347*, 631–639.

Kirkpatrick, S., Gelatt, C. D., Jr., & Vecchi, M. P. (1983) *Science 220*, 671–680.

Kraulis, P. (1991) *J. Appl. Crystallogr. 24*, 946–950.

Kühlbrandt, W., & Wang, D. N. (1991) *Nature 350*, 130–134.

Kurosaki, T., Gander, I., & Ravetch, J. V. (1991) *Proc. Natl. Acad. Sci. U.S.A. 88*, 3837–3841.

Lemmon, M. A., & Engelman, D. M. (1992) *Curr. Opin. Struct. Biol. 2*, 511–518.

Lemmon, M. A., Flanagan, J. M., Hunt, J. F., Adair, B. D., Bormann, B.-J., Dempsey, C. E., & Engelman, D. M. (1992a) *J. Biol. Chem. 267*, 7683–7689.

Lemmon, M. A., Flanagan, J. M., Treutlein, H. R., Zhang, J., & Engelman, D. M. (1992b) *Biochemistry* (preceding paper in this issue).

Manolios, N., Bonifacino, J. S., & Klausner, R. D. (1990) *Science 249*, 274–277.

Milburn, M. V., Privé, G. G., Milligan, D. L., Scott, W., Yeh, J., Jancarik, J., Koshland, D. E., Jr., & Kim, S.-H. (1991) *Science 254*, 1342–1346.

Nilges, M., & Brünger, A. T. (1991) *Protein Eng. 4*, 649–659.

Nilges, M., & Brünger, A. T. (1992) *Proteins 15*, 133–146.

O'Shea, E. K., Klemm, J. D., Kim, P. S., & Alber, T. (1991) *Science 254*, 539–544.

Pathak, D., & Sigler, P. B. (1992) *Curr. Opin. Struct. Biol. 2*, 116–123.

Popot, J.-L., & Engelman, D. M. (1990) *Biochemistry 29*, 4031–4037.

Popot, J.-L., Gerchman, S. E., & Engelman, D. M. (1987) *J. Mol. Biol. 198*, 655–676.

Richmond, T. J., & Richards, F. M. (1978) *J. Mol. Biol. 119*, 537–555.

Shoichet, B. K., & Kuntz, I. D. (1991) *J. Mol. Biol. 221*, 327–346.

Ullrich, A., & Schlessinger, J. (1990) *Cell 61*, 203–212.

Weber, I. T., & Steitz, T. A. (1987) *J. Mol. Biol. 198*, 311–326.

Welsh, E. J., & Thom, D. (1985) *Biopolymers 24*, 2301–2332.

Registry No. Gly, 56-40-6.